Mathematical Methods in the Applied Sciences

WILEY

RESEARCH ARTICLE OPEN ACCESS

Space-Time FEM Solution of Dynamic Contact Problem With Discontinuous Velocity for Multiple Impact of Deformed Bar Using PDAS Method

Victor A. Kovtunenko[1,2] | Adrien Petrov[3] | Yves Renard[3]

[1]Department of Mathematics and Scientific Computing, Karl-Franzens University of Graz, NAWI Graz, Graz, Austria | [2]Lavrentyev Institute of Hydrodynamics, Siberian Division of the Russian Academy of Sciences, Novosibirsk, Russia | [3]INSA Lyon, CNRS, Ecole Centrale de Lyon, Université Claude Bernard Lyon 1, Université Jean Monnet, ICJ UMR5208, Villeurbanne, France

Correspondence: Victor A. Kovtunenko (victor.kovtunenko@uni-graz.at)

Received: 21 August 2025 | **Revised:** 12 November 2025 | **Accepted:** 19 November 2025

Keywords: contact dynamics | deformable body impact | discontinuous velocity | semi-smooth Newton method | space-time finite element method

ABSTRACT

A class of one-dimensional impact and dynamic contact problems taking into account non-smooth velocities is studied. The new space-time finite element approximation of dynamic variational inequalities is suggested. The non-smooth solution for the impact of an obstacle by an elastic bar and its energy conservation under persistency conditions is proved on partitions of the space-time domain. The explicit solution of the double impact problem is taken as an analytical benchmark for numerical experiments. For an iterative solution, a primal-dual active set (PDAS) algorithm stemming from semi-smooth Newton methods is constructed. Numerical experiments compare the space-time PDAS method with some other existing methods: a mass redistribution method, Paoli–Schatzman scheme, and a Nitsche-based approximation, highlighting its advantages.

MSC2020 Classification: 35L85, 49M15, 74S05

1 | Introduction

In this paper, we propose a new method for space-time approximation of impact and dynamic contact problems involving non-smooth velocities. We investigate non-smooth solutions to a dynamic contact problem in a one-dimensional benchmark describing multiple impacts of a rigid obstacle by an initially deformed elastic bar, for which a periodic solution is constructed analytically. The main challenge lies in handling the discontinuities in both the velocity (i.e., time derivative of the displacement) and the spatial gradient within the weak formulation of the dynamic problem. This framework leads to a variational space-time approximation. Various discretization techniques employing continuous and discontinuous finite elements in both space and time have been described in [1–3]. For further applications of space-time methods,

we refer to [4, 5]. It is worth noting that, in the context of the wave equation, stability typically requires a CFL condition, as discussed in [6].

The existence of periodic solutions for nonlinear wave equations was established earlier in the works [7, 8]. Further mathematical results on existence for elastodynamic problems with unilateral constraints, as well as for related hyperbolic variational inequalities, are provided in [9–12]. For the approximation of elastodynamic contact problems with the help of finite element method (FEM), the reader is referred to [13]. A discrete element method for contact between deformable solids is described in [14], while advanced boundary element methods suitable for transmission and contact conditions are presented in [15]. We cite [16] for semi-analytical methods transforming the contact problem into a system of integral equations. A Petrov–Galerkin generalization of FEM, based on enrichment of trial functions, can be found in [17].

To efficiently solve complementarity problems closely related to variational inequalities, a Semi-Smooth Newton method (SSN) was proposed and implemented through the primal-dual active set (PDAS) strategy; see [18, 19]. The treatment of variational inequalities describing contact of elastic bodies and non-penetrating cracks was developed in [20, 21]. Numerical analysis and simulation of contact problems in mechanics employing the SSN can be found in [22–24]. For dynamic contact problems treated with the PDAS approach, we refer to [25, 26]. A Nitsche-based approximation relevant to elastodynamic contact is presented in [27]. More recently, Hilber–Hughes–Taylor (HHT-$\boldsymbol{\alpha}$) time-discretization schemes generalizing the Newmark family have been incorporated into the SSN method and implemented as the PDAS algorithm in [28, 29]. These methods are based on the acceleration of a field variable and consequently assume velocity continuity.

To handle discontinuous velocities, a measure-differential formulation was developed within the framework of sweeping processes in [30, 31]. It is reminiscent of a velocity-based time-stepping algorithm when reflecting the velocity, which is multiplied by a restitution coefficient, see [32]. A discontinuous second-order sweeping process in [33] addresses to contact the dynamics by employing a combination of the improved normal compliance and PDAS methods. As computational alternatives, we refer to the mass redistribution method, which is detailed for a one-dimensional elastodynamic contact problem in [34–36], and to relevant discrete time integration schemes for non-smooth impact dynamics discussed in [37]. In comparison to the time-stepping methods that are commonly used in the literature, we propose the weak formulation of time derivatives within a full space-time discretization.

As a motivation, we present an illustrative example of a vibrating unit mass on a spring, initially compressed by $u_0 < 0$ and without damping. The oscillatory behavior of the system is described by the following equation of motion:

$$\begin{cases} u_{tt}(t) + u(t) = 0 \quad \text{for } t > 0, \\ u(0) = u_0 \quad \text{and} \quad u_t(0) = 0, \end{cases} \tag{1}$$

where $u_{tt} \overset{\text{def}}{=} \frac{\mathrm{d}^2 u}{\mathrm{d}t^2}$. Note that $u(t) = u_0 \cos(t)$ is the unique solution to problem (1). The corresponding impact of the rigid obstacle $\phi = 0$ leads to the complementarity problem that can be written in the compact form as follows:

$$\begin{cases} u_{tt}(t) + u(t) = \lambda(t) \quad \text{for } t > 0, \\ 0 \geq u(t) \perp \lambda(t) \leq 0 \quad \text{for } t > 0, \\ u(0) = u_0 \quad \text{and} \quad u_t(0) = 0, \end{cases} \tag{2}$$

where the Lagrange multiplier λ implies the contact force. The orthogonality has the natural meaning: if we have enough regularity, it means that the product $u(\cdot)\lambda(\cdot)$ vanishes almost everywhere on the boundary. If we do not have enough regularity, the above inequality is integrated on an appropriate set of test functions, yielding a weak formulation for the unilateral condition. Note that (2) possesses multiple solutions given below:

$$\begin{cases} u(t) = u_0 \cos t, \quad \lambda(t) = 0 \quad \text{for } t \in \left(0, \frac{\pi}{2}\right), \\ u(t) = 0, \quad \lambda(t) < 0 \quad \text{for } t \in \mathscr{A}_k \overset{\text{def}}{=} \frac{\pi}{2} + (0, t_1) + (t_1 + \pi)k, \\ u(t) = c_k \cos\big(t + \pi(k-1) - t_1(k+1)\big), \quad \lambda(t) = 0 \quad \text{for } t \in \mathscr{I}_k \overset{\text{def}}{=} \frac{\pi}{2} + t_1 + (0, \pi) + (t_1 + \pi)k, \end{cases}$$

with arbitrary constants $t_1 > 0$ and $c_k \leq 0$, where $k \in \mathbb{N}_0$, see illustration in Figure 1. This solution is non-smooth since the velocity is discontinuous, and the acceleration is a distribution. To get the periodic solution as $c_k = u_0$ requires setting

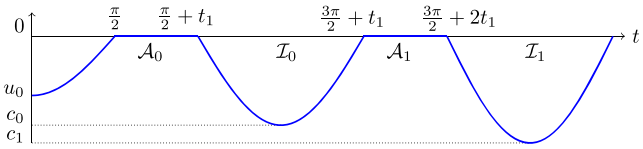

FIGURE 1 | A solution to the multiple impact of an obstacle by unit mass on a spring. [Colour figure can be viewed at wileyonlinelibrary.com]

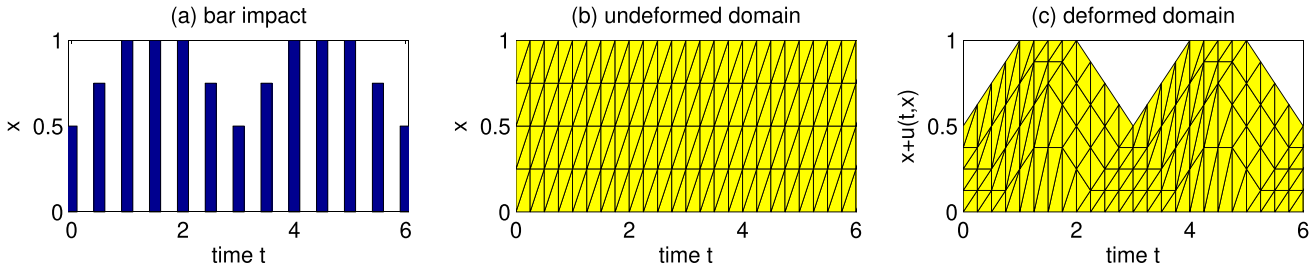

FIGURE 2 | The double impact of the rigid obstacle at $x = 1$ by an elastic bar. [Colour figure can be viewed at wileyonlinelibrary.com]

extra conditions on $\mathcal{I}_k$, where the constraint is inactive (i.e., $u \leq 0$ and $\lambda = 0$). It takes place between multiple impacts when $u = 0$ and $\lambda < 0$ corresponding to active sets $\mathcal{A}_k$. This consideration motivates our numerical regularization of the dynamic contact problem through the application of a discrete force balance at time points immediately before or after impact.

The other specialty of numerical implementation concerns the fact that the stiffness matrix for the non-smooth wave equation is generally not an M-matrix and fails to be an inverse positive. In this case, the Newton-min algorithm lacks monotone behavior and may cycle, see [38]. To remedy the monotony, we suggest a numerical procedure of reinitialization of iterates after each impact. Moreover, since the space-time discretization implies a Petrov–Galerkin FEM obeying different test and trial functions in the basis, we extend the computational domain by some fictitious time.

This paper is structured as follows. In Section 2, we formulate the one-dimensional non-smooth problem of an initially deformed elastic bar impacting a rigid obstacle from rest. A weak formulation is proposed in a primal-dual variational framework that allows discontinuous velocity profiles. An analytical solution is derived over a partition of the space-time domain, serving as a benchmark for numerical investigations. Energy conservation is ensured under persistent conditions imposed on the partition. Section 3 introduces the space-time discretization of this benchmark problem using uniform triangular meshes and piecewise-linear polynomials. For the iterative solution, we employ the PDAS algorithm and provide insights into addressing the monotonicity of active sets and achieving super-linear convergence. Numerical tests in Section 4 investigate the displacement field computed on the contact boundary, energy conservation, and a-posteriori convergence to the analytical solution in the energy norm when decreasing the mesh size parameters. Comparative results with the known, highly efficient methods show that our approach offers significant advantages and potential for further improvement. Moreover, the sensitivity of the space-time discretization to variation of the geometry, when exact times of impact do not coincide with grid points at the contact boundary, is investigated. In this case, we propose addressing the issue using a mass redistribution technique. The decomposition into sub-PDAS procedures is discussed in Section 5.

2 | Variational Formulation for the Impact Problem

We consider an elastic bar of length L under tension-compression, with unit mass density and unit elastic modulus. More precisely, one end of the bar is free to move as long as it does not hit a material obstacle, while the other end is clamped (see Figure 2a).

We now present the mathematical formulation of the problem. The bar is assumed to be made of a homogeneous material and to obey the theory of small deformations. Let x denote the spatial coordinate along the bar, with the origin located

at the material obstacle. Let $u(t,x)$ represent the displacement at time $t \in [0,T]$, $T>0$, of the material point located at position $x \in [0,L]$. The mathematical problem is then formulated as follows:

$$u_{tt}(t,x) - u_{xx}(t,x) = 0 \quad \text{for } (t,x) \in (0,T)\times(0,L), \tag{3}$$

with Cauchy initial data

$$u(0,x) = u_0(x) \quad \text{and} \quad u_t(0,x) = v_0(x), \tag{4}$$

where $u_t \overset{\text{def}}{=} \frac{\partial u}{\partial t}$ and $u_x \overset{\text{def}}{=} \frac{\partial u}{\partial x}$. We assume that the bar is fixed at one end $x=0$, and impacts the rigid obstacle $\phi = 0$ at the other end $x=L$. The impact is described by pointwise complementarity conditions at the contact boundary:

$$0 \geq u(t,L) \perp \lambda(t) \leq 0 \quad \text{for } t \in (0,T). \tag{5}$$

In the smooth case of continuously differentiable functions, the contact force λ can be determined from the balance of normal reaction:

$$\lambda(t) = u_x(t,L) \quad \text{for } t \in (0,T). \tag{6}$$

We assume that the initial displacement $u_0 \in \mathrm{H}^1(0,L)$ in the Sobolev space and satisfies the compatibility conditions, that is $u_0(0)=0$ and $u_0(L) \leq 0$ and the initial velocity $v_0 \in \mathrm{L}^2(0,L)$. Let us describe the weak formulation associated with our problem. To this aim, we introduce the following sets:

$$\begin{aligned}
\mathrm{H}^1_{0,}(0,T) &\overset{\text{def}}{=} \{v \in \mathrm{H}^1(0,T) \,:\, v(0)=0\},\\
\mathrm{H}^1_{,0}(0,T) &\overset{\text{def}}{=} \{v \in \mathrm{H}^1(0,T) \,:\, v(T)=0\},\\
\mathrm{V}_{0,} &\overset{\text{def}}{=} \mathrm{L}^2(0,T;\mathrm{H}^1_{0,}(0,L)) \cap \mathrm{H}^1_{0,}(0,T;\mathrm{L}^2(0,L)),\\
\mathrm{V}_{,0} &\overset{\text{def}}{=} \mathrm{L}^2(0,T;\mathrm{H}^1_{0,}(0,L)) \cap \mathrm{H}^1_{,0}(0,T;\mathrm{L}^2(0,L)).
\end{aligned}$$

The former set $\mathrm{V}_{0,}$ has zeros on the bottom and left faces of the space-time domain, while the latter $\mathrm{V}_{,0}$ has zeros on the bottom and right faces of the space-time domain. Then, the weak formulation associated to problem (3–5) is obtained by multiplying (3) by $v-u$ and by integrating formally this result over $Q_T \overset{\text{def}}{=} (0,T)\times(0,L)$, we get

$$\begin{cases}
\text{Find } u-u_0 \in \mathrm{V}_{0,} \text{ such that } u(t,L) \leq 0 \text{ for } t \in (0,T),\\
\int_{Q_T} \left(-u_t(v_t-u_t) + u_x(v_x-u_x)\right)\,\mathrm{d}x\,\mathrm{d}t \geq \int_0^L v_0(v(0,\cdot)-u_0)\,\mathrm{d}x\\
\text{for all } v-u \in \mathrm{V}_{,0} \text{ with } v(t,L) \leq 0 \text{ for } t \in (0,T).
\end{cases} \tag{7}$$

The unique solvability to (7) is proved in [35]. For the H^2-smooth solution u, the problem (7) follows the wave Equation (3), the Lagrange multiplier λ in (6), and the initial velocity $u_t(0,\,\cdot) = v_0$.

With the help of Lagrange multiplier (the dual variable), the variational inequality (7) can be written in the primal-dual form as dynamic LCP:

$$\begin{cases}
\text{Find } u-u_0 \in \mathrm{V}_{0,} \text{ and } \lambda \in \mathrm{L}^2(0,T) \text{ such that}\\
u(\cdot\,,L) \leq 0, \quad \lambda \leq 0, \quad \int_0^T \lambda u(\cdot\,,L)\,\mathrm{d}t = 0 \text{ and}\\
\int_{Q_T}(-u_t v_t + u_x v_x)\,\mathrm{d}x\,\mathrm{d}t - \int_0^T \lambda v(\cdot\,,L)\,\mathrm{d}t = \int_0^L v_0 v(0,\,\cdot)\,\mathrm{d}x \quad \text{for all } v \in \mathrm{V}_{,0}.
\end{cases} \tag{8}$$

It is worth noting that the gradient u_x on the contact boundary at $x=L$ associated to λ by (6) in general is determined as a distribution only. We justify non-smooth solutions to (8) based on the following construction.

Assume partition without overlapping of the rectangle $Q_T = \bigcup_{i=1}^N \overline{K}_i$ into polygons K_i with boundaries ∂K_i and outward normal vectors $\mathbf{n}^i$. In the interior $\mathrm{int}(Q_T)$, denote by Γ_{ij} the straight edge joining K_i and K_j for $j \neq i$ with the normal $\mathbf{n}^{ij}$ pointed from K_i into K_j as illustrated in Figure 3.

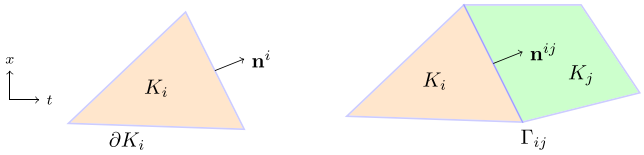

FIGURE 3 | One element K_i, and two joint elements K_i and K_j in a partition. [Colour figure can be viewed at wileyonlinelibrary.com]

Introducing the jump of a discontinuous field $\phi(t,x)$ over the edge:

$$[\![\phi]\!] \overset{\text{def}}{=} \phi|_{\partial K_j \cap \Gamma_{ij}} - \phi|_{\partial K_i \cap \Gamma_{ij}},$$

We adapt Green's formula on the partition to get

$$\sum_{i=1}^{N} \int_{K_i} (u_{tt} - u_{xx})\,\mathrm{d}x\,\mathrm{d}t = \sum_{i=1}^{N} \int_{K_i} (-u_t v_t + u_x v_x)\,\mathrm{d}x\,\mathrm{d}t + \sum_{\overline{K}_i \cap \{t=0,T\}} \int_{\partial K_i \cap \{x \in (0,L)\}} u_t n_1^i\,\mathrm{d}x$$
$$- \sum_{\overline{K}_i \cap \{x=0,L\}} \int_{\partial K_i \cap \{t \in (0,T)\}} u_x n_2^i\,\mathrm{d}t + \sum_{\Gamma_{ij} \cap \mathrm{int}(Q_T)} \int_{\Gamma_{ij}} [\![(-u_t n_1^{ij} + u_x n_2^{ij}) v]\!]\,\mathrm{d}\Gamma, \tag{9}$$

which holds for discontinuous fields u_t, u_x, v, that are smooth within each element K_i.

Theorem 2.1. *Let a piecewise, twice continuously differentiable, $u(t,x)$ and a piecewise continuous $\lambda(t)$ fulfill the following relations on the partition*:

$$\begin{cases} u_{tt} - u_{xx} = 0 \text{ in } K_i \text{ for } i = 1, \dots, N, \\ -[\![u_t]\!] n_1^{ij} + [\![u_x]\!] n_2^{ij} = 0 \text{ on } \Gamma_{ij} \in \mathrm{int}(Q_T), \\ u = 0 \text{ on } \partial K_i \cap \{x = 0\} \text{ and } 0 \geq u \perp \lambda \leq 0 \text{ on } \partial K_i \cap \{x = L\}, \\ u = u_0 \text{ and } u_t = v_0 \text{ on } \partial K_i \cap \{t = 0\}. \end{cases} \tag{10}$$

Then it justifies the non-smooth solution to (8).

Proof. Theorem 2.1 follows directly from Green's formula (9), applied to test functions $v \in \mathrm{V}_{,0}$ that are continuous and satisfy $[\![v]\!] = 0$. The Lagrange multiplier $\lambda = u_x(\cdot, L)$ is identified via the force balance condition (6). □

Let us define energy of the bar on the partition:

$$E(s) \overset{\text{def}}{=} \frac{1}{2} \sum_{K_i \cap \{t=s\}} \int_{K_i \cap \{t=s,\ x \in (0,L)\}} (u_t^2 + u_x^2)\,\mathrm{d}x \text{ for all } s \in (0,T). \tag{11}$$

The physical model is characterized by its conservation of energy.

Theorem 2.2. *If solution to problem* (10) *satisfies the persistency conditions on the partition*:

$$\begin{cases} [\![\frac{1}{2}(u_t^2 + u_x^2) n_1^{ij} - u_t u_x n_2^{ij}]\!] = 0 \text{ on } \Gamma_{ij} \in \mathrm{int}(Q_T), \\ \sum\limits_{\overline{K}_i \cap \{x=L\}} \int_{\partial K_i \cap \{t \in (0,T)\}} u_x u_t\,\mathrm{d}t = 0, \end{cases} \tag{12}$$

then the energy is conserved, that is $E(t) = E(0)$ for all $t \in [0,T]$.

Proof. From Green's formula (9) (without integration by parts over time) applied to the non-smooth solution u of (10) and discontinuous test function $v = u_t$ in the moving domain Q_s, thanks to equations in (10) we have:

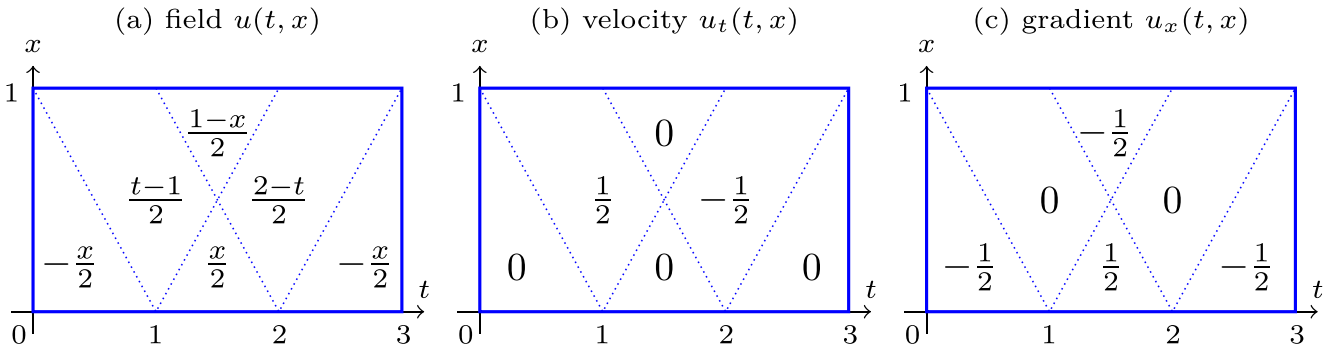

FIGURE 4 | Analytical solution for periodic impact: Displacement (a); velocity (b); gradient (c). [Colour figure can be viewed at wileyonlinelibrary.com]

$$0 = \sum_{K_i} \int_{K_i \cap \{t<s\}} (u_{tt} - u_{xx}) u_t \, \mathrm{d}x \, \mathrm{d}t = \sum_{K_i} \int_{K_i \cap \{t<s\}} \left(\frac{1}{2}(u_t^2)_t + u_x u_{tx} \right) \mathrm{d}x \, \mathrm{d}t$$
$$- \sum_{\overline{K}_i \cap \{x=L\}} \int_{\partial K_i \cap \{t \in (0,s)\}} u_x u_t \, \mathrm{d}t + \sum_{\Gamma_{ij}} \int_{\Gamma_{ij} \cap \mathrm{int}(Q_s)} [\![u_x n_2^{ij} u_t]\!] \, \mathrm{d}\Gamma,$$

where $u_t = 0$ at $x = 0$ was used. Integrating by parts over time with the help of assumptions (12) it follows:

$$0 = \frac{1}{2} \left(\sum_{K_i} \int_{K_i \cap \{t<s\}} (u_t^2 + u_x^2)_t \, \mathrm{d}x \, \mathrm{d}t + \sum_{\Gamma_{ij}} \int_{\Gamma_{ij} \cap \mathrm{int}(Q_s)} [\![(u_t^2 + u_x^2) n_1^{ij}]\!] \, \mathrm{d}\Gamma \right)$$
$$= E(s) - E(0),$$

which proves the theorem. □

Following Theorem 2.1, we construct explicitly a time-periodic solution to the impact problem (8) in a particular case corresponding to that in [34]. Namely, let $L = 1$, the initial field $u_0 = -x/2$ and velocity $v_0 = 0$. For the period $T = 3$, the analytical solution reads:

$$u(t,x) = \begin{cases} -\frac{x}{2} & \text{for } t \geq 0,\ t + x \leq 1, \\ \frac{t-1}{2} & \text{for } 1 \leq t + x \leq 2,\ t - x \leq 1, \\ \frac{x}{2} & \text{for } 1 \leq t + x \leq 2,\ t - x \geq 1, \\ \frac{1-x}{2} & \text{for } t + x \geq 2,\ t - x \leq 1, \\ \frac{2-t}{2} & \text{for } t + x \geq 2,\ 1 \leq t - x \leq 2, \\ -\frac{x}{2} & \text{for } t - x \geq 2,\ t \leq 3. \end{cases}$$

The solution u, its velocity u_t, and its gradient u_x are shown on Figure 4.

It is worth noting that both the velocity and the spatial gradient exhibit discontinuities in space and time on the partition into six elements. The persistency condition (12) holds because of $u_t^2 + u_x^2 = 0.25$ is constant and $u_t u_x = 0$ in every element. Consequently, by Theorem 2.2, the energy of the bar given in (11), is constant over time and equal to $E(t) = 0.125$. This non-smooth solution will be used as a benchmark for numerical analysis in the next section.

3 | Numerical Resolution of an Impact Problem

We introduce the space-time discretization on regular triangular meshes $\mathcal{T}_h$, see an example in Figure 2b, given by standard piecewise-linear polynomials:

$$\mathrm{V}^h \overset{\mathrm{def}}{=} \left\{ v_h \in C^0([0,T] \times [0,L]),\ v_h|_K \in \mathbb{P}_1(K) \text{ for all } K \in \mathcal{T}_h,\ v_h(\cdot\,,0) = 0 \right\},$$

respectively for trial and test functions:

$$\mathrm{V}^h_{0,} \overset{\text{def}}{=} \{v_h \in \mathrm{V}^h,\ v_h(0,\ \cdot) = 0\}, \quad \mathrm{V}^h_{,0} \overset{\text{def}}{=} \{v_h \in \mathrm{V}^h,\ v_h(T,\ \cdot) = 0\}.$$

The basis functions $\phi_0, \dots, \phi_{\mathrm{DOF}} \in \mathrm{V}^h$ in the space-time domain are given by standard piecewise-linear "hat"-functions on a 6-point patch of triangles. Here, DOF is the number of degrees of freedom. The triangular elements are employed to align with characteristics $x + t = \text{const}$ and $x - t = \text{const}$ of the wave equation.

Let the mesh $\mathcal{T}_h$ on the contact boundary at $x = L$ be represented by distinct time points $0 = t^0 < t^1 < \cdots < t^M = T$ with $\tau_m \overset{\text{def}}{=} t^m - t^{m-1}$. The discontinuous gradient $u_{hx}(\cdot\ , L)$ of a function $u_h \in \mathrm{V}^h$ is piecewise constant on the partition $[0, T] = \bigcup_{m=1}^M \overline{T}_m$, where $T_m \overset{\text{def}}{=} (t^{m-1}, t^m)$, given by the trace:

$$u_{hx}(\cdot\ , L)|_{T_m} = u_{hx}|_K \text{ for } K \in \mathcal{T}_h \text{ such that } t^{m-1}, t^m \in K.$$

Then the integral over the contact boundary for the $\mathbb{P}_1$-approximation reads:

$$\int_0^T u_{hx} v_h \ \mathrm{d}t|_{x=L} = \sum_{m=1}^M u_{hx}(\cdot\ , L)|_{T_m} \frac{v_h(t^{m-1}, L) + v_h(t^m, L)}{2} \tau_m, \tag{13}$$

for functions $u_h, v_h \in \mathrm{V}^h$.

Using (13) and introducing the discrete Lagrange multiplier intended to represent the contact stress on intervals according to (6), we set the space-time discretized variational problem (8) in the form:

$$\begin{cases} \text{Find } u_h - u_{0h} \in \mathrm{V}^h_{0,} \text{ and } \lambda_h \in \mathbb{R}^M \text{ such that on } T_m \text{ we have} \\ u_h|_{T_m} \le 0, \quad \lambda_m \le 0, \quad \displaystyle\sum_{m=1}^M \lambda_m \tau_m \frac{u_h(t^{m-1}, L) + u_h(t^m, L)}{2} = 0, \\ \displaystyle\int_{Q_T} (-u_{ht} v_{ht} + u_{hx} v_{hx}) \ \mathrm{d}x \ \mathrm{d}t - \int_0^L v_{0h} v_h(0,\ \cdot) \ \mathrm{d}x \\ \quad = \displaystyle\sum_{m=1}^M \lambda_m \tau_m \frac{v_h(t^{m-1}, L) + v_h(t^m, L)}{2} \quad \text{for all } v_h \in \mathrm{V}^h_{,0}, \end{cases} \tag{14}$$

where u_{0h} (respectively v_{0h}) is an approximation in V^h of the field u_0 (respectively, the initial velocity v_0 at $t = 0$). Reducing λ_h from (14), it can be expressed as the discretized variational inequality (7). We construct its solution using the iterative procedure described below.

Let us order the first $\phi_0, \dots, \phi_M$ "hat"-basis functions on $\mathcal{T}_h$ with nonzero support on the contact boundary such that $\phi_m(t^n, L) = \delta_{mn}$. We test equations in (14) by $v_h = \phi_m \in \mathrm{V}^h_{,0}$ and define residuals $r_0, \dots, r_{M-1} \in \mathbb{R}$ as follows:

$$r_m \overset{\text{def}}{=} \int_{Q_T} (-u_{ht} \phi_{mt} + u_{hx} \phi_{mx}) \ \mathrm{d}x \ \mathrm{d}t - \int_0^L v_{0h} \phi_m(0,\ \cdot) \ \mathrm{d}x. \tag{15}$$

Then (14) follows equations for $r_h \in \mathbb{R}^M$:

$$r_0 = \frac{\lambda_1 \tau_1}{2} \text{ and } r_m = \frac{\lambda_m \tau_m + \lambda_{m+1} \tau_{m+1}}{2},$$

which can be inverted for $\lambda_h \in \mathbb{R}^M$ recursively via the residual:

$$\lambda_1 = \frac{2 r_0}{\tau_1}, \quad \lambda_{m+1} = \frac{2 r_m - \lambda_m \tau_m}{\tau_{m+1}} \quad \text{for } m = 1, \dots, M - 1. \tag{16}$$

The representation of Lagrange multipliers in (16) is advantageous since it does not employ any regularity assumptions on the solution.

The complementarity conditions on $T_1, \dots, T_M$ in (14) can be expressed as nonlinear equations:

$$\lambda_m = \min\left(0, \lambda_m - \frac{u_h(t^{m-1}, L) + u_h(t^m, L)}{2}\right), \tag{17}$$

provided by the same sign of $u_h(t^{m-1}, L), u_h(t^m, L)$ on T_m. Indeed, if $\lambda_m - (u_h(t^{m-1}, L) + u_h(t^m, L))/2 \geq 0$, then $\lambda_m = 0$ follows $u_h(t^{m-1}, L) + u_h(t^m, L) \leq 0$. Otherwise, $\lambda_m - (u_h(t^{m-1}, L) + u_h(t^m, L))/2 < 0$ yields $u_h(t^{m-1}, L) + u_h(t^m, L) = 0$ and $\lambda_m < 0$. According to (17) we define active and inactive intervals T_m:

$$\begin{cases} \mathcal{A}(u_h, \lambda_h) \overset{\text{def}}{=} \left\{ \operatorname{int}\left(\bigcup \overline{T}_m\right) : \ \lambda_m - \frac{u_h(t^{m-1}, L) + u_h(t^m, L)}{2} < 0 \right\}, \\ \mathcal{I}(u_h, \lambda_h) \overset{\text{def}}{=} \left\{ \bigcup \overline{T}_m : \ \lambda_m - \frac{u_h(t^{m-1}, L) + u_h(t^m, L)}{2} \geq 0 \right\}, \end{cases} \tag{18}$$

such that either $u_h(t, L) = 0$ for $t \in T_m$ as $T_m \subset \mathcal{A}(u_h, \lambda_h)$, or $\lambda_m = 0$ for complementary $T_m \subset \mathcal{I}(u_h, \lambda_h)$. Using active and inactive sets given in (18) the following complementarity problem stems from (14):

$$\begin{cases} \text{Find } u_h - u_{0h} \in \mathrm{V}^h_{0,} \text{ and } \lambda_h \in \mathbb{R}^M \text{ such that on } T_m \text{ we have} \\ u_h = 0 \text{ on } \mathcal{A}(u_h, \lambda_h), \quad \lambda_h = 0 \text{ on } \mathcal{I}(u_h, \lambda_h), \\ \displaystyle\int_{Q_T} (-u_{ht} v_{ht} + u_{hx} v_{hx}) \, \mathrm{d}x \, \mathrm{d}t - \int_0^L v_{0h} v_h(0, \cdot) \, \mathrm{d}x \\ \quad = \displaystyle\sum_{m=1}^{M} \lambda_m \tau_m \frac{v_h(t^{m-1}, L) + v_h(t^m, L)}{2} \quad \text{for all } v_h \in \mathrm{V}^h_{,0}. \end{cases} \tag{19}$$

The PDAS algorithm iterates (19) over active sets and employs residuals from (15), (16) as follows.

Algorithm 3.1 (space-time PDAS). **Initialization step**: *Initialize active set* $\mathcal{A}^0 = \emptyset$ *and inactive set* $\mathcal{I}^0 = [0, T]$, *set iteration number* $k = 0$.

Iteration step: *Solve the linear system of equations on the linear subspace*:

$$\begin{cases} \textit{Find } u_h^k - u_{0h} \in \mathrm{V}^h_{0,} \textit{ such that} \quad u_h^k = 0 \textit{ on } \mathcal{A}_h^k, \\ \displaystyle\int_{Q_T} (-u_{ht}^k v_{ht} + u_{hx}^k v_{hx}) \, \mathrm{d}x \, \mathrm{d}t - \int_0^L v_{0h} v_h(0, \cdot) \, \mathrm{d}x = 0 \\ \textit{for all } v_h \in \mathrm{V}^h_{,0} \textit{ with } v_h = 0 \textit{ on } \mathcal{A}_h^k, \end{cases} \tag{20}$$

where v_h *are spanned by the basis functions* ϕ_h *that belong to the linear subspace. Compute the residual* $r_h^k \in \mathbb{R}^M$ *and Lagrange multiplier* $\lambda_h^k \in \mathbb{R}^M$:

$$\begin{cases} r_h^k = \displaystyle\int_{Q_T} (-u_{ht}^k \phi_{ht} + u_{hx}^k \phi_{hx}) \, \mathrm{d}x \, \mathrm{d}t - \int_0^L v_{0h} \phi_h(0, \cdot) \, \mathrm{d}x, \\ \lambda_1^k = \dfrac{2 r_0^k}{\tau_1}, \quad \lambda_{m+1}^k = \dfrac{2 r_m^k - \lambda_m^k \tau_m}{\tau_{m+1}} \quad \textit{for } m = 1, \dots, M-1. \end{cases} \tag{21}$$

Update active and inactive sets:

$$\begin{cases} \mathcal{A}_h^{k+1} = \left\{ \operatorname{int}\left(\bigcup \overline{T}_m\right) : \ \lambda_m^k - \frac{u_h^k(t^{m-1}, L) + u_h^k(t^m, L)}{2} < \texttt{tol} \right\}, \\ \mathcal{I}_h^{k+1} = \left\{ \bigcup \overline{T}_m : \ \lambda_m^k - \frac{u_h^k(t^{m-1}, L) + u_h^k(t^m, L)}{2} \geq \texttt{tol} \right\}, \end{cases} \tag{22}$$

Termination step: *Exit if* $\mathcal{A}^{k+1} = \mathcal{A}^k$ *or cycling, else increase iteration number* $k = k + 1$ *and go to the iteration step.*

The unique solvability of space-time discretized variational problems for linear wave equations (20) can be found in [6]. The behavior of the PDAS algorithm that is attained is demonstrated in Figure 5.

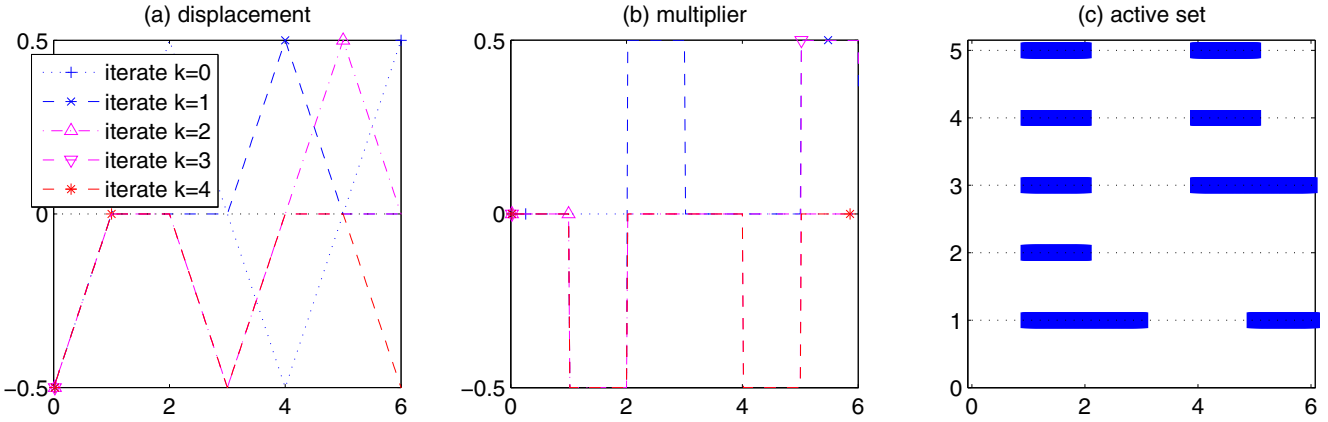

FIGURE 5 | PDAS iterates: displacement $u_h^k(t,1)$ (a); multiplier $\lambda_h^k(t,1)$ (b); active set $\mathcal{A}_h^k$ (c). [Colour figure can be viewed at wileyonlinelibrary.com]

Here the displacement $u_h^k(t,1)$ (left), Lagrange multiplier $\lambda_h^k(t,1)$ (center), and active set $\mathcal{A}_h^k$ (right) are depicted along the contact boundary with $M = 300$ time points. The algorithm terminates as $\mathcal{A}_h^5 = \mathcal{A}_h^4$ in only $k = 0, \dots, 4$ iterates at the discrete solution $(u_h^4, \lambda_h^4) = (u_h, \lambda_h)$ to the dynamic impact problem (19). Below we hint (i)–(iv) to the implementation of the generic Algorithm 3.1.

i. To avoid numerical instabilities caused by grazing contact when the both variables u_m^k and λ_m^k are almost zeros on T_m, we use a small tolerance $\texttt{tol} = -10^{-5}$ to split between active and inactive sets in (22).

ii. Since the linear span of the basis functions in the trial space $\mathrm{V}_{0,}^h$ differs from the test space $\mathrm{V}_{,0}^h$ at initial $t = 0$ and final $t = T$ times, we extend $t^0, \dots, t^M$ by two fictitious time steps t^{M+1} and t^{M+2} composing one additional patch. In the extended computation domain $(0, t^{M+2}) \times (0, L)$, test functions $v_h = 0$ at $t = t^{M+2}$, and they agree trial functions at $t = T$. In the extension we impose the inactive condition $\lambda_m = 0$ in (6) hold pointwise for $m = M+1, M+2$:

$$u_{hx}(t^m, L) = 0. \tag{23}$$

In practice, the stiffness matrix at a fixed iterate is expressed in the reduced form as follows:

$$\begin{cases} M_{11}u_h(t^m, L) + M_{12}u_h(t^m, L-h) = F_1, \\ M_{21}u_h(t^m, L) + M_{22}u_h(t^m, L-h) = F_2, \end{cases}$$

The first equation is replaced according to (23) by

$$u_h(t^m, L) - u_h(t^m, L-h) = 0.$$

For redistribution in (26), the second equation is then replaced by:

$$(M_{11} + M_{21})u_h(t^m, L) + (M_{12} + M_{22})u_h(t^m, L-h) = F_1 + F_2.$$

iii. Since the stiffness matrix associated with the non-smooth wave equation is generally not an M-matrix, we propose reinitializing (22) with inactive intervals in order to remedy the monotonic behavior of the PDAS algorithm iterates.

$$\tilde{\mathcal{A}}_h^{k+1} \overset{\text{def}}{=} \mathcal{A}_h^{k+1} \cap \mathcal{A}_h^k \text{ and } \tilde{\mathcal{I}}_h^{k+1} \overset{\text{def}}{=} \bigcup \overline{T}_m \setminus \mathcal{A}_h^{k+1}$$

at that the iteration k where repeated active sets increase:

$$\left(\mathcal{A}_h^{k+1} \cap \mathcal{A}_h^k\right) \supset \left(\mathcal{A}_h^k \cap \mathcal{A}_h^{k-1}\right).$$

The purpose of this strategy is to preserve the active sets over time and to avoid fluctuations. An example of such reinitialization at Iterations 2 and 4 is illustrated in Figure 5c. Following the first impact at iteration for $k = 1$ (setting $\mathcal{A}_h^{-1} = \emptyset$), the sets $\mathcal{A}_h^2$ and complementary $\mathcal{I}_h^2$ in (22) were replaced by reinitialized ones $\tilde{\mathcal{A}}_h^2$ and $\tilde{\mathcal{I}}_h^2$, then the iteration step continued. The next reinitialization occurred at $k = 3$, following the second impact.

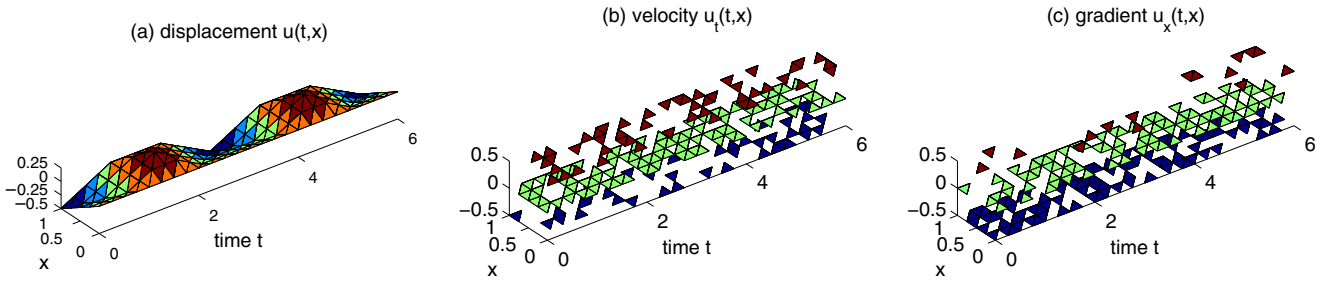

FIGURE 6 | Discrete solution as $N = 4$: displacement u_h (a); velocity u_{ht} (b); gradient u_{hx} (c). [Colour figure can be viewed at wileyonlinelibrary.com]

iv. To treat multiple impacts (more than one), motivated by the example of non-uniqueness in the Introduction, we impose pointwise condition (23) exceptionally at that times $t^m = t^{m^*-1}$ on the inactive intervals T_{m^*} which are followed by the active intervals T_{m^*+1}. The reason is to keep the force balance violated here when setting $t^{m^*} = 0$.

In the following section, we validate the behavior of Algorithm 3.1 on the benchmark given in Figure 4 and compare it with other numerical schemes.

4 | Benchmark for the Double Impact Problem

A uniform space-time mesh is generated over the rectangular domain $Q = (0, 6) \times (0, 1)$, as depicted in Figure 2 (b). For integer N, we set the mesh size $h = 1/N$ equal to the step size $\tau = 6/N$ for $M = 6N$ time points. The double impact problem (19) is computed numerically using the PDAS algorithm. For $N = 4$, the algorithm converged successfully after 5 iterations. The resulting discrete solution is shown in Figure 6, displaying the displacement field $u_h(t, x)$ (left), the velocity field $u_{ht}(t, x)$ (center), and the gradient field $u_{hx}(t, x)$ (right). The corresponding deformed domain $(t, x + u(t, x))$ for $(t, x) \in Q$ is shown in Figure 2c.

Our analysis focuses on the discrete displacement $u_h(t, 1)$ at the contact boundary for $t \in (0, 6)$, and on the discrete energy E_h, evaluated via the following formula:

$$E_m = \frac{1}{2} \sum_{K \in \mathcal{T}_h \cap \{t=t^m\}} \int_{K \cap \{t=t^m,\ x \in (0,1)\}} (u_{ht}^2 + u_{hx}^2)\, \mathrm{d}x, \tag{24}$$

as well as the relative energy error, expressed in percents:

$$\mathrm{Err}_h = \frac{h}{E} \sqrt{\sum_{m=1}^{M} (E_m - E)^2} \times 100\%, \tag{25}$$

where the exact energy $E = 1/8$. The numerical results corresponding to (19), (24), and (25) are shown, respectively, in the left, center, and right panels of Figure 7 for $N \in \{10, 20, 30, 40, 50\}$, which correspond to mesh sizes $h = 0.1, 0.05, 0.03, 0.025, 0.02$, respectively. In the left plot, we observe that numerical values in grid points are visually indistinguishable from the exact solution even on the coarse mesh. The energy plot in the center exhibits some bounded piecewise constant behavior. From the right plot, we may conclude with a super-linear convergence of the solution as $h \to 0$ in the energy norm. No oscillations are observed.

For comparison, we consider three of the most efficient methods reported in the literature: the Nitsche-based Verlet time integration method from [27], the restitution coefficient based method proposed by Paoli and Schatzman [39], and the mass redistribution method introduced in [36].

In Figure 8, the numerical solution by Nitsche-based Verlet method is presented for N space points of mesh size $h = 1/N$ and $M = 14N$ time points of step size $\tau = 3h/7$ that is required to satisfy CFL condition. For the values

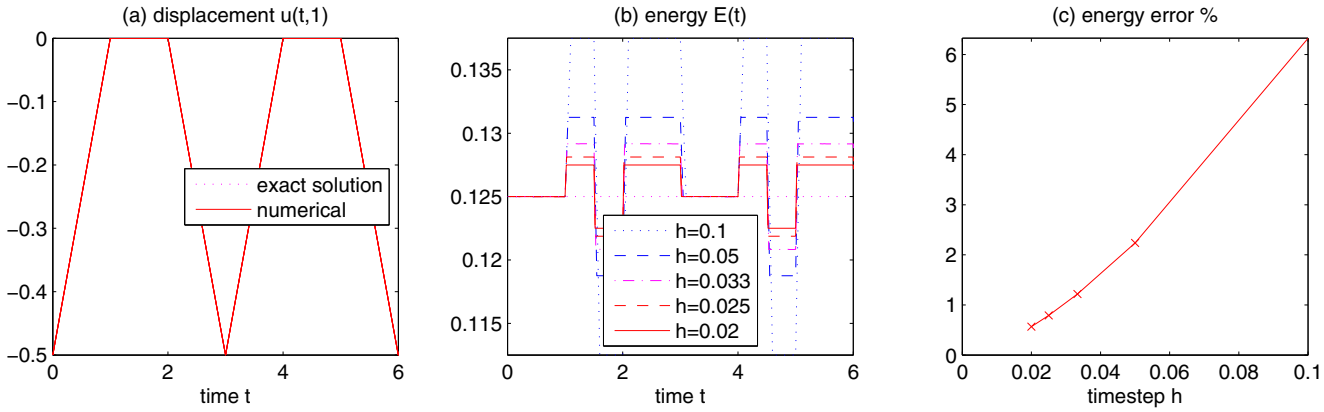

FIGURE 7 | Discrete displacement $u_h(\cdot\,,1)$ (a); energy E_h (b); energy error Err_h (c). [Colour figure can be viewed at wileyonlinelibrary.com]

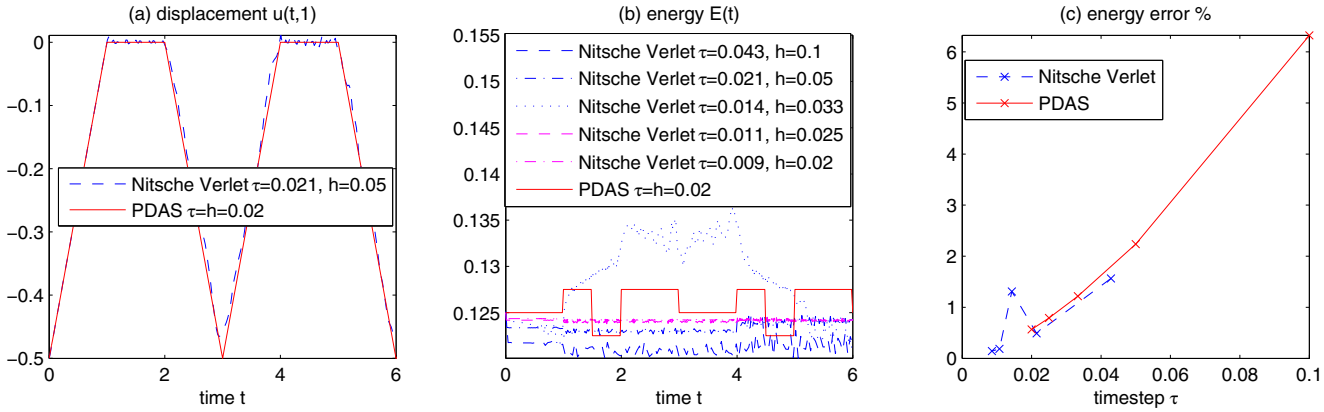

FIGURE 8 | Nitsche–Verlet method: displacement $u_h(\cdot\,,1)$ (a); energy E_h (b); error Err_h (c). [Colour figure can be viewed at wileyonlinelibrary.com]

$N \in \{10, 20, 30, 40, 50\}$ with $h = 0.1, 0.05, 0.03, 0.025, 0.02$ and $\tau \approx 0.043, 0.021, 0.014, 0.011, 0.009$, the discrete displacement $u_h(t, 1)$ at the contact boundary (left), discrete energy E_h (center), and the relative energy error Err_h (right) are depicted in Figure 8 in comparison with the numerical solution by PDAS method. In the left plot, we clearly observe that PDAS provides a more accurate approximation of the displacement at the contact boundary for comparable mesh sizes h and τ. The center and right plots show that the Nitsche–Verlet method offers a slightly better approximation of the energy; however, it exhibits instability (notably at $N = 30$) and spurious oscillations.

A similar comparison with the restitution method is illustrated in Figure 9. The displacement $u_h(\cdot\,,1)$ obtained using the restitution-based method exhibits no oscillations but remains less accurate than the PDAS solution, as shown in the left plot. The center and right plots further indicate that the PDAS method yields a more accurate approximation of the energy E_h, as measured by Err_h, for comparable time steps τ.

Figure 10 shows the numerical solution computed by the mass redistribution method for the same discretization parameters as before. It is compared with the discrete solution of (19) computed by Algorithm 3.1 with respect to the error in the maximum norm as well as in the energy norm in (24) and (25). Once again, all three plots confirm the superior accuracy of the PDAS method. We remark that the largest inaccuracies in the Nitsche–Verlet, restitution, and mass redistribution methods occur at the singular time $t = 3$ when the velocity changes at the contact boundary from $u_{ht}(t, 1) = -0.5$ for $t < 3$ to $u_{ht}(t, 1) = 0.5$ for $t > 3$.

It is worth noting that, although the discrete contact boundary is aligned with the impact times, the space-time mesh does not align with the discontinuities that propagate along the characteristic lines $x + t = \text{const}$ and $x - t = \text{const}$ inside

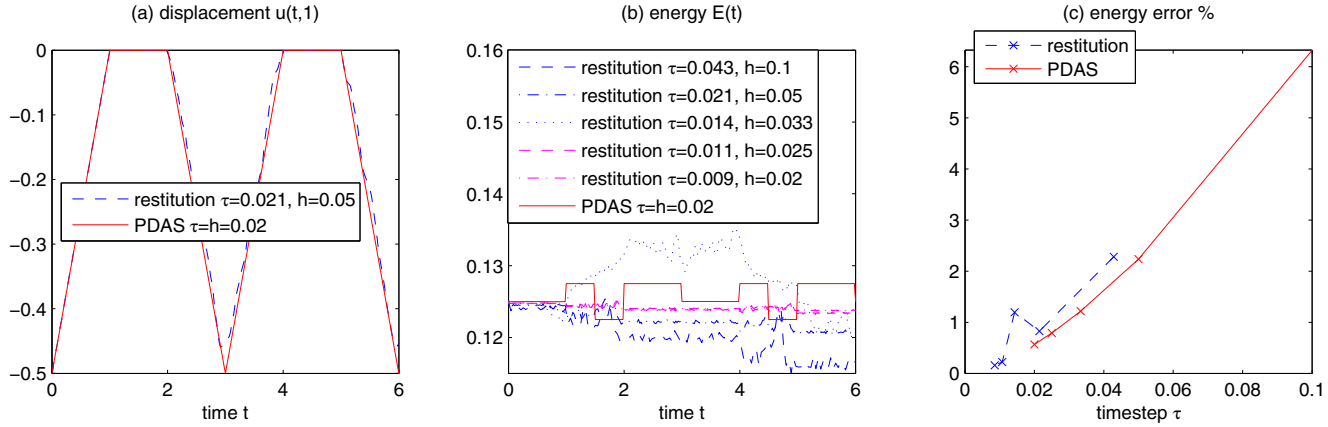

FIGURE 9 | Restitution-based method: displacement $u_h(\cdot\,,1)$ (a); energy E_h (b); error Err_h (c). [Colour figure can be viewed at wileyonlinelibrary.com]

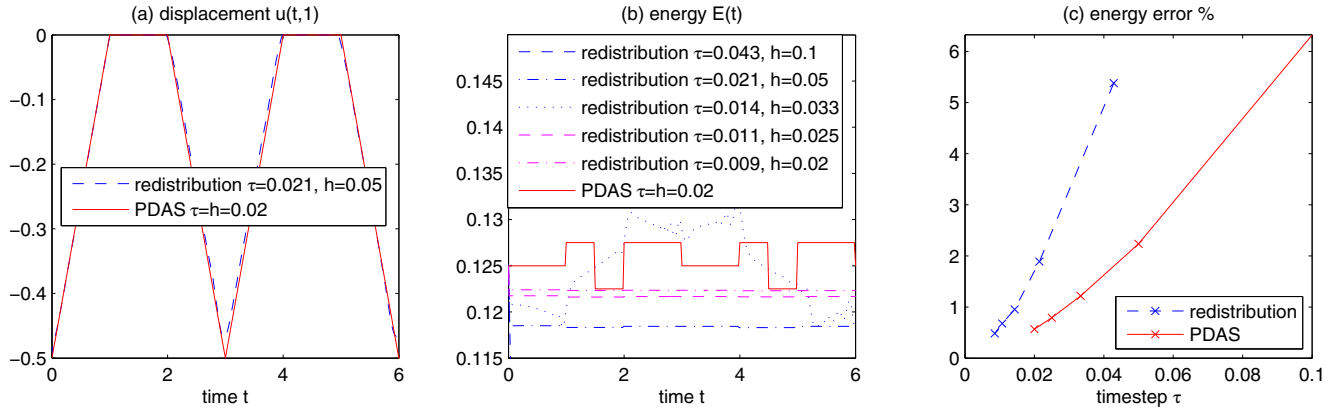

FIGURE 10 | Redistribution method: displacement $u_h(\cdot\,,1)$ (a); energy E_h (b); error Err_h (c). [Colour figure can be viewed at wileyonlinelibrary.com]

the domain (see Figure 4). As a result, the exact solution does not lie within the finite element approximation space. In order to investigate this effect in more detail, we perturb the characteristics by $x + \varkappa t = \text{const}$ and $x - \varkappa t = \text{const}$. In this setting, the exact impact times no longer coincide with the mesh points at the contact boundary. To this end, we introduce a perturbation to the wave Equation (3) by

$$u_{tt} - \varkappa^2 u_{xx} = 0 \quad \text{in } Q,$$

with $\varkappa = 0.99$ close to 1. The observed instability indicates a lack of convergence in the iteration process. To ensure convergence of the PDAS iterations, we enforce the inactive condition (23) at the inactive time points t^m:

$$u_h(t^m, 1) = u_h(t^m, 1 - h). \tag{26}$$

In doing so, the mass is redistributed by transferring the stiffness contributions from the inactive boundary at $x = 1$ to the corresponding nodes at $x = 1 - h$. In three plots of Figure 11 the corresponding displacement $u_h(\cdot\,,1)$, energy E_h, and energy error Err_h are depicted. In this case, spurious oscillations can be seen in the center plot, and a slight instability can be observed in the right plot, in comparison with Figure 7. However, the displacement at the contact boundary, shown in the left plot, remains free of oscillations and is indistinguishable from the analytical solution, even at the singular time.

5 | Decomposition Into Sub-PDAS Procedures

Another important aspect involves decomposing the problem in sub-PDAS procedures by splitting the rectangle $Q = \bigcup_{n=1}^{S} Q_n$ into $S \geq 1$ subsequent time sub-domains $Q_n := (t_{n-1}, t_n) \times (0,1)$ by points $0 = t_0 < \cdots < t_S = T$. This

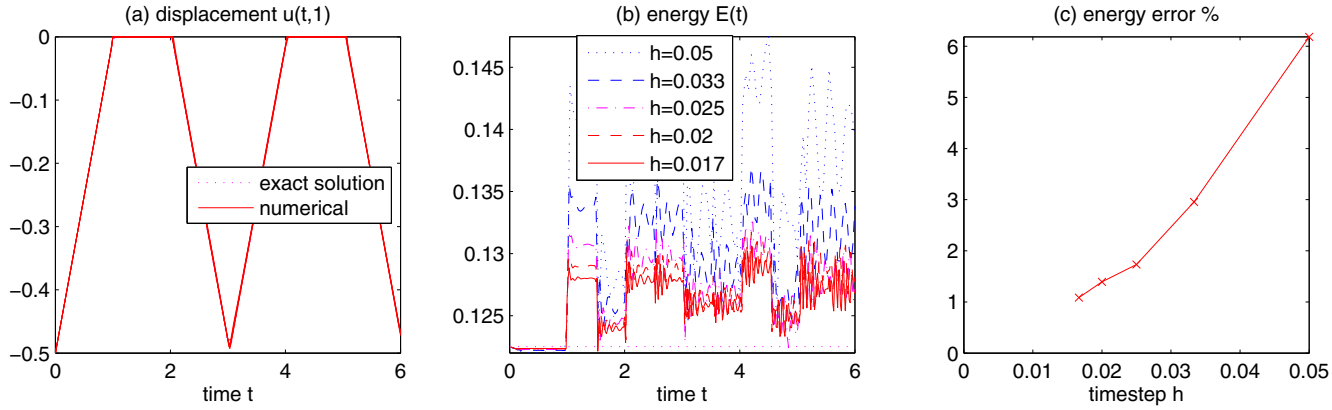

FIGURE 11 | Perturbed by $\varkappa = 0.99$ displacement $u_h(\cdot\,, 1)$ (a); energy E_h (b); error Err_h (c). [Colour figure can be viewed at wileyonlinelibrary.com]

TABLE 1 | Sub-PDAS procedure by split into equal time sub-domains for $N = 50$. Total number of iterations and the maximum difference with respect to the non-splitted procedure.

# Sub-domains	1	2	3	4
# Iterates	7	8	8	11
% Difference	0	2×10^{-12}	4×10^{-12}	2×10^{-12}

approach requires a space-time mesh that is conforming to the decomposition; that is, no elements crossed by the lines $t = t_i$ for $i = 1, \ldots, S-1$. Such a strategy could make the scheme competitive even for 3D problems, where it may be advantageous to assign one sub-domain per time step.

We perform this decomposition into sub-PDAS procedures through successive partial solves of the displacement and contact multipliers over the sub-domains Q_1 to Q_S. In each sub-domain Q_n, the relevant displacement degrees of freedom are those associated with nodes for which $t_{n-1} < t \leq t_n$, as the displacement at $t = t_{n-1}$ is already determined in either Q_{n-1} or by the initial condition. The multiplier degrees of freedom involved are those whose shape function supports lie within Q_n. Finally, the solution within each sub-domain Q_n is computed using the equations associated with displacement test functions being the shape functions whose nodes satisfy $t_{n-1} \leq t < t_n$, in accordance with the Petrov–Galerkin strategy.

A typical result of numerical experiments is presented in Table 1 for $N = 50$, where Q is split into $S = 1, 2, 3, 4$ sub-domains, with the equidistant time points $t_n = 6n/S$, $n = 0, \ldots, S$. The difference compared to the PDAS procedure without decomposition is on the order of machine precision, confirming that the decomposition does not affect the numerical solution. The increase in the number of PDAS iterations remains moderate and is offset by the reduced size of the individual systems being solved.

6 | Conclusion

We propose in this work a new method for space-time approximation of impact and dynamic contact problems involving non-smooth velocities. Discontinuous Galerkin methods employ a similar approach for time integration, as discussed in [40]. Our implementation is based on the PDAS iterative approach. We tested the method on a one-dimensional benchmark problem of double impact, for which an explicit analytical solution is available. From numerical experiments, we observe that the solution obtained using the space-time PDAS algorithm coincides with the analytical solution at grid points, particularly at singular time points when the non-smooth velocity changes at the contact boundary. The solution error, measured in the integral norm of energy, primarily arises from the piecewise-linear approximation within the elements. This error can be improved through the use of specifically structured grids, such as crisscross or adaptive meshing. The energy is non-dissipative and presented by a piecewise constant line. Certainly advantageous is the

fact that the numerical solution is free of spurious oscillations. For further development, multidimensional problems are foreseen.

Author Contributions

Victor A. Kovtunenko: conceptualization. **Adrien Petrov:** writing – review and editing. **Yves Renard:** validation.

Acknowledgments

Victor A. Kovtunenko is supported by the OeAD Scientific & Technological Cooperation (MULT 06/2023) financed by the Austrian Federal Ministry of Science, Research and Economy (BMWFW). Adrien Petrov and Yves Renard are supported by the Ministry for Europe and Foreign Affairs (France) within Programme Danube 2023-2025 (Project PHC Danube no49916UM). The open access is provided by the University of Graz. Open Access funding provided by Universitat Graz/KEMÖ.

Funding

This study was supported by OeAD GmbH - Austria's Agency for Educaton and Internatonalisaton (MULT_06/2023) and Ministère de l'Europe et des Affaires Étrangères (PHC_Danube_no49916UM).

Conflicts of Interest

The authors declare no conflicts of interest.

Data Availability Statement

The authors have nothing to report.

References

1. H. Blum, T. Jansen, A. Rademacher, and K. Weinert, "Finite Elements in Space and Time for Dynamic Contact Problems," *International Journal for Numerical Methods in Engineering* 76, no. 10 (2008): 1632–1644, https://doi.org/10.1002/nme.2389.

2. G. M. Hulbert and T. J. R. Hughes, "Space-Time Finite Element Methods for Second-Order Hyperbolic Equations," *Computer Methods in Applied Mechanics and Engineering* 84, no. 3 (1990): 327–348, https://doi.org/10.1016/0045-7825(90)90082-W.

3. G. R. Richter, "An Explicit Finite Element Method for the Wave Equation," *Applied Numerical Mathematics* 16, no. 1–2 (1994): 65–80, https://doi.org/10.1016/j.cam.2018.06.030.

4. C. Hager and B. Wohlmuth, "Analysis of a Space-Time Discretization for Dynamic Elasticity Problems Based on Mass-Free Surface Elements," *SIAM Journal on Numerical Analysis* 47, no. 3 (2009): 1863–1885, https://doi.org/10.1137/080715627.

5. P. Junker and T. Wick, "Space-Time Variational Material Modeling: A New Paradigm Demonstrated for Thermo-Mechanically Coupled Wave Propagation, Visco-Elasticity, Elasto-Plasticity With Hardening, and Gradient-Enhanced Damage," *Computational Mechanics* 73, no. 2 (2024): 365–402, https://doi.org/10.1007/s00466-023-02371-2.

6. O. Steinbach and M. Zank, "Coercive Space-Time Finite Element Methods for Initial Boundary Value Problems," *Electronic Transactions on Numerical Analysis* 52 (2020): 154–194, https://doi.org/10.1553/etna_vol52s154.

7. E. Feireisl, "Weakly Damped Quasilinear Wave Equation: Existence of Time-Periodic Solutions," *Nonlinear Analysis: Theory Methods & Applications* 17, no. 8 (1991): 711–723, https://doi.org/10.1016/0362-546X(91)90208-I.

8. P. I. Plotnikov, "Existence of a Countable Set of Periodic Solutions of the Problem of Forced Oscillations for a Weakly Nonlinear Wave Equation," *Mathematics of the USSR-Sbornik* 64, no. 2 (1989): 543–556, https://doi.org/10.1070/SM1989v064n02ABEH003327.

9. T. Kashiwabara and H. Itou, "Unique Solvability of a Crack Problem With Signorini-Type and Tresca Friction Conditions in a Linearized Elastodynamic Body," *Philosophical Transactions of the Royal Society A* 380, no. 2236 (2022): 20220225, https://doi.org/10.1098/rsta.2022.0225.

10. S. Migórski, W. Han, and S. Zeng, "A New Class of Hyperbolic Variational–Hemivariational Inequalities Driven by Non-Linear Evolution Equations," *European Journal of Applied Mathematics* 32, no. 1 (2021): 59–88, https://doi.org/10.1017/S0956792520000030.

11. A. Petrov and M. Schatzman, "Mathematical Results on Existence for Viscoelastodynamic Problems With Unilateral Constraints," *SIAM Journal on Mathematical Analysis* 40, no. 5 (2009): 1882–1904, https://doi.org/10.1137/070695101.

12. E. M. Rudoy and S. A. Sazhenkov, "The Homogenized Dynamical Model of a Thermoelastic Composite Stitched With Reinforcing Filaments," *Philosophical Transactions A* 382, no. 2277 (2024): 20230304, https://doi.org/10.1098/rsta.2023.0304.

13. F. Chouly, P. Hild, and Y. Renard, *Finite Element Approximation of Contact and Friction in Elasticity* (Birkhäuser, 2023), https://doi.org/10.1007/978-3-031-31423-0.

14. N. Dirani and L. Monasse, "An Explicit Pseudo-Energy Conservative Scheme for Contact Between Deformable Solids," *International Journal for Numerical Methods in Engineering* 125, no. 4 (2023): e7395, https://doi.org/10.1002/nme.7395.

15. J. Gwinner and E. P. Stephan, *Advanced Boundary Element Methods. Treatment of Boundary Value, Transmission and Contact Problems* (Springer, 2018), https://doi.org/10.1007/978-3-319-92001-6.

16. M. Yaylac, M. Yayl, Ş. Öztürk, et al., "Examining the Contact Problem of a Functionally Graded Layer Supported by an Elastic Half-Plane With the Analytical and Numerical Methods," *Mathematical Methods in the Applied* 47 (2024): 10400–10420, https://doi.org/10.1002/mma.10129.

17. V. A. Kovtunenko and K. Kunisch, "Revisiting Generalized FEM: A Petrov–Galerkin Enrichment Based FEM Interpolation for Helmholtz Problem," *Calcolo* 55, no. 3 (2018): 38, https://doi.org/10.1007/s10092-018-0280-5.

18. M. Bergounioux, K. Ito, and K. Kunisch, "Primal-Dual Strategy for Constrained Optimal Control Problems," *SIAM Journal on Control and Optimization* 37, no. 4 (1999): 1176–1194, https://doi.org/10.1137/S0363012997328609.

19. M. Hintermüller, V. A. Kovtunenko, and K. Kunisch, "Generalized Newton Methods for Crack Problems With Non-Penetration Condition," *Numerical Methods for Partial Differential Equations* 21, no. 3 (2005): 586–610, https://doi.org/10.1002/num.20053.

20. A. M. Khludnev and V. A. Kovtunenko, *Analysis of Cracks in Solids* (WIT-Press, 2000).

21. V. A. Kovtunenko, "Numerical Simulation of the Non-Linear Crack Problem With Non-Penetration," *Mathematical Methods in the Applied Sciences* 27 (2004): 163–179, https://doi.org/10.1002/mma.449.

22. M. Hintermüller, V. A. Kovtunenko, and K. Kunisch, "Constrained Optimization for Interface Cracks in Composite Materials Subject to Non-Penetration Conditions," *Journal of Engineering Mathematics* 59, no. 3 (2007): 301–321, https://doi.org/10.1007/s10665-006-9113-7.

23. M. Hintermüller, V. A. Kovtunenko, and K. Kunisch, "A Papkovich–Neuber-Based Numerical Approach to Cracks With Contact in 3D," *IMA Journal of Applied Mathematics* 74, no. 3 (2009): 325–343, https://doi.org/10.1093/imamat/hxp017.

24. W. Wang, H. Xuan, X. Cheng, and K. Liang, "Numerical Analysis and Simulation of a Quasistatic Frictional Bilateral Contact Problem With Damage, Long-Term Memory and Wear," *Computers and Mathematics With Applications* 177 (2025): 130–146, https://doi.org/10.1016/j.camwa.2024.11.020.

25. M. Barboteu, F. Bonaldi, S. Dumont, and C. Mahmoud, "An Energy-Consistent Discretization of Hyper-Viscoelastic Contact Models for Soft Tissues," *Computer Methods in Applied Mechanics and Engineering* 421, no. 5 (2024): 116785, https://doi.org/10.1016/j.cma.2024.116785.

26. S. Hartmann, S. Brunssen, E. Ramm, and B. Wohlmuth, "Unilateral Non-Linear Dynamic Contact of Thin-Walled Structures Using a Primal-Dual Active Set Strategy," *International Journal for Numerical Methods in Engineering* 70, no. 8 (2007): 883–912, https://doi.org/10.1002/nme.1894.

27. F. Chouly and Y. Renard, "Explicit Verlet Time-Integration for a Nitsche-Based Approximation of Elastodynamic Contact Problems," *Advanced Modeling and Simulation in Engineering Sciences* 5 (2018): 31, https://doi.org/10.1186/s40323-018-0124-5.

28. V. A. Kovtunenko and Y. Renard, "FEM Approximation of Dynamic Contact Problem for Fracture Under Fluid Volume Control Using HHT-α and Semi-Smooth Newton Methods," *Applied Numerical Mathematics* 218 (2025): 148–158, https://doi.org/10.1016/j.apnum.2025.07.009.

29. V. A. Kovtunenko and Y. Renard, "Convergence Analysis of Semi-Smooth Newton Method for Mixed FEM Approximations of Dynamic Two-Body Contact and Crack Problems," *Journal of Computational and Applied Mathematics* 471 (2026): 116722, https://doi.org/10.1016/j.cam.2025.116722.

30. M. Jean, "The Non-Smooth Contact Dynamics Method," *Computer Methods in Applied Mechanics and Engineering* 177, no. 3–4 (1999): 235–257, https://doi.org/10.1016/S0045-7825(98)00383-1.

31. J. J. Moreau, "Numerical Aspects of the Sweeping Process," *Computer Methods in Applied Mechanics and Engineering* 177, no. 3–4 (1999): 329–349, https://doi.org/10.1016/S0045-7825(98)00387-9.

32. R. Dzonou, M. D. P. Monteiro Marques, and L. Paoli, "A Convergence Result for a Vibro-Impact Problem With a General Inertia Operator," *Nonlinear Dynamics* 58, no. 1–2 (2009): 361–384, https://doi.org/10.1007/s11071-009-9484-1.

33. V. A. T. Nguyen, S. Abide, M. Barboteu, and S. Dumont, "An Improved Normal Compliance Method for Non-Smooth Contact Dynamics," in *Nonsmooth Problems With Applications in Mechanics*, vol. 127, ed. S. Migórski and M. Sofonea (Banach Center Publications, 2024), 191–217, https://doi.org/10.4064/bc127-9.

34. F. Dabaghi, P. Krejčí, A. Petrov, J. Pousin, and Y. Renard, "A Weighted Finite Element Mass Redistribution Method for Dynamic Contact Problems," *Journal of Computational and Applied Mathematics* 345, no. 8 (2019): 338–356, https://doi.org/10.1016/j.cam.2018.06.030.

35. F. Dabaghi, A. Petrov, J. Pousin, and Y. Renard, "A Robust Finite Element Redistribution Approach for Elastodynamic Contact Problems," *Applied Numerical Mathematics* 103 (2016): 48–71, https://doi.org/10.1016/j.apnum.2015.12.004.

36. H. B. Khenous, P. Laborde, and Y. Renard, "Comparison of Two Approaches for the Discretization of Elastodynamic Contact Problems," *Comptes Rendus De L'academie Des Sciences. Serie I, Mathematique* 342, no. 10 (2006): 791–796, https://doi.org/10.1016/j.crma.2006.03.011.

37. J. Di Stasio, D. Dureisseix, A. Gravouil, G. Georges, and T. Homolle, "Benchmark Cases for Robust Explicit Time Integrators in Non-Smooth Transient Dynamics," *Advances in Modeling and Simulation in Engineering Sciences* 6, no. 2 (2019): 1–31, https://doi.org/10.1186/s40323-019-0126-y.

38. I. Ben Gharbia and J. C. Gilbert, "Nonconvergence of the Plain Newton-Min Algorithm for Linear Complementarity Problems With a P-Matrix," *Mathematical Programming* 134, no. 2 (2012): 349–364, https://doi.org/10.1007/s10107-010-0439-6.

39. L. Paoli and M. Schatzman, "A Numerical Scheme for Impact Problems I: The One-Dimensional Case," *SIAM Journal on Numerical Analysis* 40, no. 2 (2002): 702–733, https://doi.org/10.1137/S0036142900378728.

40. T. Schindler and V. Acary, "Timestepping Schemes for Nonsmooth Dynamics Based on Discontinuous Galerkin Methods: Definition and Outlook," *Mathematics and Computers in Simulation* 95 (2014): 180–199, https://doi.org/10.1016/j.matcom.2012.04.012.